OMNY PIN—A versatile sample holder for tomographic measurements at room and cryogenic temperatures

M. Holler,[1] J. Raabe,[1] R. Wepf,[2,a)] S. H. Shahmoradian,[1] A. Diaz,[1] B. Sarafimov,[1] T. Lachat,[3] H. Walther,[1] and M. Vitins[1,b)]
[1]*Paul Scherrer Institut, 5232 Villigen PSI, Switzerland*
[2]*Scientific Center for Optical and Electron Microscopy ScopeM, ETH Zurich, 8093 Zürich, Switzerland*
[3]*EnDes Engineering Partner AG, 4703 Kestenholz, Switzerland*

(Received 14 July 2017; accepted 29 October 2017; published online 20 November 2017)

Nowadays ptychographic tomography in the hard x-ray regime, i.e., at energies above about 2 keV, is a well-established measurement technique. At the Paul Scherrer Institut, currently two instruments are available: one is measuring at room temperature and atmospheric pressure, and the other, the so-called OMNY (tOMography Nano crYo) instrument, is operating at ultra-high vacuum and offering cryogenic sample temperatures down to 10 K. In this manuscript, we present the sample mounts that were developed for these instruments. Aside from excellent mechanical stability and thermal conductivity, they also offer highly reproducible mounting. Various types were developed for different kinds of samples and are presented in detail, including examples of how specimens can be mounted on these holders. We also show the first hard x-ray ptychographic tomography measurements of high-pressure frozen biological samples, in the present case *Chlamydomonas* cells, the related sample pins and preparation steps. For completeness, we present accessories such as transportation containers for both room temperature and cryogenic samples and a gripper mechanism for automatic sample changing. The sample mounts are not limited to x-ray tomography or hard x-ray energies, and we believe that they can be very useful for other instrumentation projects. https://doi.org/10.1063/1.4996092

I. INTRODUCTION

X-ray computed tomography (CT) is widely used in imaging as it allows three-dimensional visualization of specimens non-destructively.[1] For a measurement, many projections of a specimen are acquired from different sample orientations and reconstructed into a three-dimensional dataset. Ideally, the projections are equally distributed in angles in the range from 0° to 180°. In cases where the entire range is not accessible, a so-called missing wedge occurs, which leads to reconstruction artifacts and non-isotropic 3D resolution.[2] Therefore, a sample should ideally be accessible from all sides when rotating around one axis. X-ray computed tomography can provide resolution in the micrometer range and is performed in many laboratories and also at synchrotron light sources.[3] With new developments, resolution is continuously improved to sub-micrometer scale, and 3D images of tiny objects have become possible.[4] More and more nano x-ray imaging modalities, instrumentation, and data processing schemes are explored and scientifically applied worldwide,[5,6] even at cryogenic sample conditions.[7–12] In our case, we are using ptychographic x-ray computed tomography.[13] Here, the individual projections are acquired by scanning a sample in a confined coherent x-ray beam such that consecutive illuminated areas partially overlap, and far-field diffraction patterns are recorded at each scanning position. The overlapping exposure creates data with enough diversity such that iterative phase retrieval algorithms converge in a robust way, retrieving the sample's complex-valued transmissivity and illumination, i.e., the method provides absorption and phase contrast.[14] In contrast to other scanning techniques, the resolution in ptychography is determined by the largest angle at which the diffraction patterns can be reliably measured and not by the size of the illumination, and thus the resolution can be orders of magnitude smaller than the beam size. However, the sample has to be positioned in the beam with accuracy better than the target resolution. To facilitate accurate positioning, we developed tracking laser interferometry compatible with scanning and rotation[15] that is implemented in the setup described in detail elsewhere.[16,17] This metrology requires a flat and spherical mirror to be close to the sample. In order to minimize residual thermal drift, the measurement dead path, i.e., the distance between the sample and mirror, was minimized. This was achieved by converting the reference mirror itself to the receptor for the sample pins. The sample pins described in Sec. II provide the required mechanical stability for scanning microscopy in the nanometer resolution range. In the cryogenic variant of this instrument, the so-called OMNY (tOMography Nano crYo) endstation, cryogenic cooling of the sample is achieved via heat conduction, i.e., the reference mirror/sample holder is connected to a cryostat and cooled down, thereby removing heat from the sample pins.

a)Current address: Centre for Microscopy & Microanalysis, University of Queensland, 4072 St. Lucia Queensland, Australia.
b)Current address: RUAG Schweiz AG, RUAG Schweiz AG, 8052 Zürich, Switzerland.

We therefore developed a versatile sample pin for nanotomography measurements of samples with dimensions ranging from 1 μm to hundreds of micrometers that can simplify sample handling and preparation. Several variants of this system have been developed for different types of samples and requirements. The holders allow for measurements at room temperature but are optimized for measurements at cryogenic conditions. Various manufacturing drawings are provided as supplementary material. As an example of a technical challenge resolved by these pins, we further show a demonstration of nanotomography of high pressure frozen *Chlamydomonas* cells with a resolution of about 100 nm in 3D. We expect that such pin designs can be used in other setups aiming for high-resolution nanotomography or pre-aligned sample exposure both for room and cryogenic temperatures.

II. OMNY PIN

All variants of the OMNY pin share the same receptor and therefore have a common base geometry as depicted in Fig. 1(a). All dimensions in the drawings are shown in millimeters. The conical area (1) with a half-cone angle of 2° functions as the holding surface. Mounting is achieved by pushing the pin into the matching pin receptor as depicted in Fig. 1(b). In our case, the pin receptor is manufactured from either stainless steel for general-purpose use, or of aluminum, which provides better thermal conductivity for cryogenic experiments. The pins are manufactured from oxygen-free copper (OFHC) for optimized thermal conductivity. The cone creates high surface forces when mounting such that the thermal contact area between the pin and receptor is increased compared to other mechanisms, such as spring-driven holders. To avoid cold welding effects between the pin and receptor, the pins are coated with a 3 μm-thick gold layer.

The conical shape has proven to be mechanically stable; projection measurements with sub-10 nm resolution have been successfully performed, and an isotropic 3D resolution below 15 nm has been demonstrated[18] in the instrument measuring at room temperature.[16,17] These results were limited in resolution by mechanical stability of the entire setup and available photon flux, not by the sample pin. The sample position itself is in all pin variants located 3 mm above the upper pin surface [Fig. 1(a-3), red dot] and is centered to the axis of the pin. An advantageous side effect of the conical pin shape is the automatic centering of the pin axis to the pin receptor, such that the radial mounting and axial mounting are very reproducible, allowing one to quickly locate and align samples for a measurement.

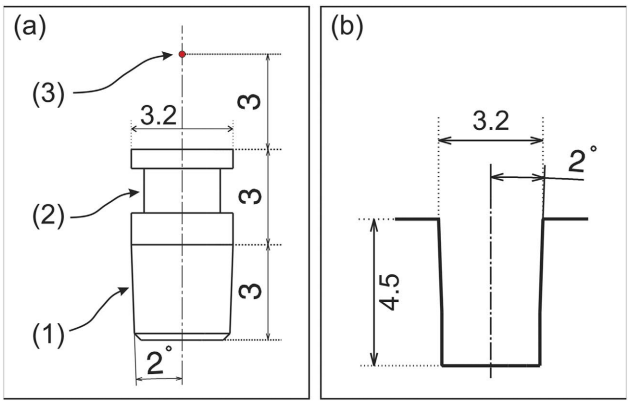

FIG. 1. (a) Basic OMNY pin geometry (1) conical mounting base, (2) handling area, (3) measurement position. (b) The matching pin receptor where the OMNY pin is simply inserted for mounting.

For the handling of the pins, it is important that the conical region will not be damaged. Therefore, a gripping area has been introduced [Fig. 1(a-2)] in which the pins can be reliably grabbed by tweezers or automatic sample-changing robots. The fact that the conical area cannot be clamped in more traditional sample holders creates the difficulty in mounting such pins in other instruments, which is important for enabling correlative imaging, for example. Therefore, to make the pins compatible with other devices, a pin adaptor has been designed that converts the conical shape to a 3 mm cylinder that can be screw clamped in the typical standard sample mounts used in many instruments (see also Sec. II A).

Various variants of the pin have been developed and are described in Subsections II A–II D. Depending on how samples are mounted to the pins, it is possible to re-use them. This is especially easy when using glue that can be removed by solvents. However, in our case, we typically use the pins one-way, especially because samples are typically archived after measurements. This keeps the possibility to look at a sample again at a later point.

A. Tip version

The tip version of the OMNY pin is depicted in Figs. 2(a)–2(c) and provides a sharp tip in which samples can be mounted. This version is ideal if pillars of a sample are prepared by focused ion-beam milling. Such samples are typically extracted using a micromanipulator as available in FIB/SEM machines and then glued to the tip of the OMNY pin using the deposition system in the FIB/SEM. An example is depicted in Fig. 3, showing how the pin is inserted in the adaptor [Fig. 3(a)] and then screw-clamped into the holder of the FIB/SEM machine [Fig. 3(b)]. The sample is prepared and attached to a micromanipulator [Fig. 3(c)], extracted and mounted on top of the pin, and finally detached from the micromanipulator [Fig. 3(d)]. Examples of measurements performed on samples mounted using this method can be found in Refs. 18–23.

It is also possible to manually glue samples to the pin using adhesives. In this case, the sample either has to possess the appropriate dimensions prior to mounting, as for example in Refs. 24 and 25, which may be the natural case, or can be achieved by milling in a FIB/SEM or laser ablation system. Such trimming could also be done after manual mounting on the tip, as was done in Ref. 26. For gluing samples directly, it has proven beneficial to file down the tip of such pins and create a flat platform matching the dimensions of the sample. Such a mounting platform can be created by gently sliding polishing paper with grain sized of a few microns over the tip. Figure 4 shows an example where a sample pillar with an 80% undercut has been created in a FIB/SEM and then glued to the pin using a micromanipulator external of the FIB/SEM which avoids the

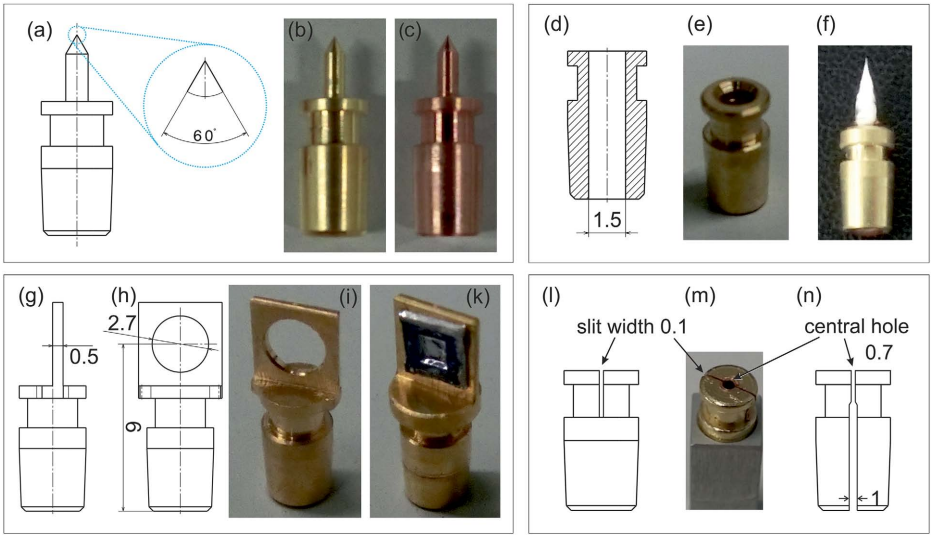

FIG. 2. Different variants of the OMNY pin. [(a)–(c)] The tip version, [(d)–(f)] glass capillary version, [(g)–(k)] for 2D samples, [(l)–(n)] copper tube version for high-pressure frozen suspensions.

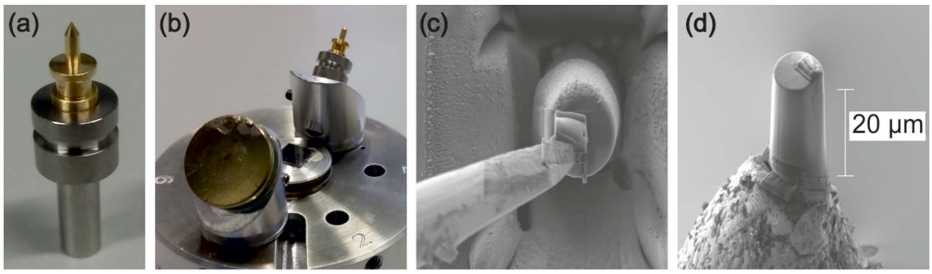

FIG. 3. Mounting a sample in a FIB/SEM. (a) The pin in the adaptor converting to a cylindrical shaft to screw clamp it in the typical mounts available in FIB/SEM machines (b). (c) The SEM image of a sample prepared in the FIB/SEM and attached to a micromanipulator. (d) SEM image of the sample mounted on the pin.

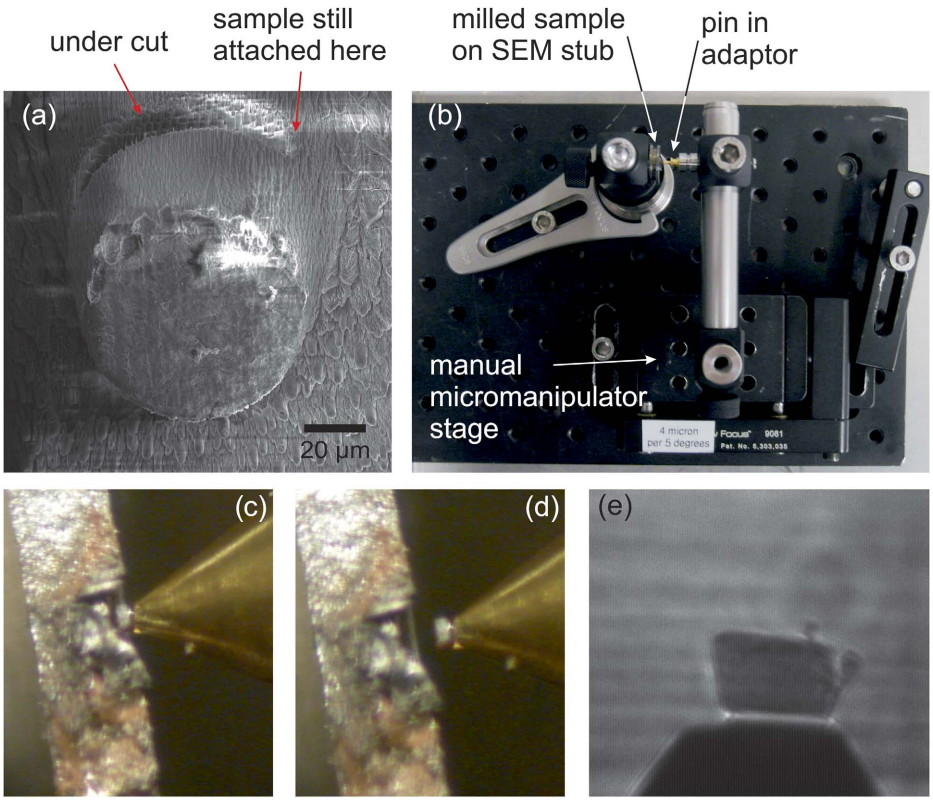

FIG. 4. Preparing a sample in FIB/SEM and mounting manually outside the FIB/SEM. (a) SEM image of an 80 μm diameter pillar below of which an undercut was created with a depth about 80% of its diameter. (b) The SEM stub with the milled sample was mounted on a breadboard and approached by a filed down pin with matching tip diameter. A little amount of adhesive was applied to the tip which was brought to contact with the sample using a manual micromanipulator. (c) A light microscopy view of the pin in contact with the sample. (d) After the glue was cured, the sample was ripped off the stub by cracking the remaining sample area. (e) X-ray micrograph of the sample on top of the pin ready for a tomographic measurement.

transfer process in the FIB/SEM. After preparing the sample [Fig. 4(a)], the entire SEM stub was mounted on a breadboard. The diameter of the pillar prepared in the present case was 80 μm. Epoxy adhesive (Araldite) was applied to the tip of the pin which was mounted on a pin adaptor on a micromanipulator stage (Newport 9081, five axis aligner) as shown in Fig. 4(b). The pin was approached to the sample [Fig. 4(c)], and after the glue was cured, the sample was ripped from its surrounding area [Fig. 4(d)]. Figure 4(e) shows an x-ray micrograph of the mounted sample on top of the pin as it could be used for tomography.

The tip version is also suited for preparing cryogenically fixed samples of biological tissue as has been demonstrated in Ref. 27. Here, biological tissue that was infiltrated with cryo-protectant was placed on the tip of a filed pin and then gradually frozen to −90 °C in a cryo-ultramicrotome chamber. After freezing, the sample was trimmed to the appropriate dimensions for a measurement using a diamond knife in the cryo-ultramicrotome, which was equipped with a pin adaptor.

B. Glass capillaries

For samples such as pastes or powders, the tip version is not well suited. However, such samples can be often inserted into a tapered glass capillary. Tapered capillaries can be fabricated with a capillary puller; in our case, Sutter Instrument P-2000 is used, providing a smallest diameter of approximately 4 μm. Figures 2(d) and 2(e) show an OMNY pin that was designed for this case. The hollow pin offers an inner diameter of 1.5 mm and a glass capillary containing the sample can be inserted and fixed by adhesives. Figure 2(f) shows such a holder with a mounted capillary. To ensure a reproducible measurement position, we developed the following procedure. Figure 5 shows a mounting device that allows for accurate positioning of tapered glass capillaries into the hollow pin. A light microscope mounted on a manual xyz translation stage allows for observing the tip position of the pin that is determined by the position of a pin receptor mounted at a fixed place. Though this microscope provides a view from the side, it provides the 3D position of the sample when combined with the depth of focus. Typically a 10× magnification (10× Mitutoyo Plan Apo, depth of focus 3.5 μm) allows for the capillary tip to be centered with a 10-μm precision. This simplifies the alignment of samples and enables precise centering as required for our cases.[15] For centering a capillary, the position of the microscope itself is first calibrated using a tip-version OMNY pin. Then, a hollow pin is mounted, and a glass capillary is inserted. Controlled curing is achieved by using a UV curing adhesive (Norland Products, Inc., NOA 81). This permits the manipulation of the capillary until the region of interest is found at the measurement position in the microscope. Manipulation of the capillary is achieved from the capillary end that protrudes from the bottom of the pin and rests on a holder mounted on a manual xy stage. The capillary end typically extends to about 30–50 mm, depending on the length of the original capillary before pulling. The glue is then cured, which finalizes the mounting process with an optional cutting of the capillary protruding at the end of the pin with a diamond glass cutter. Examples of measurements of samples in glass capillaries can be found in Refs. 28–30.

C. Flat samples

For samples that need to be mounted on a two-dimensional support, tomographic measurements with a missing angular wedge can still be performed, as explained in the Introduction. Figures 2(g)–2(k) show the corresponding pin. Figure 2(k) shows a Si_3N_4 membrane with test structures glued to such a pin. The measurement area is relatively large, and in some cases it can be useful to have the sample at a lower position. Therefore, we created two variants of this mount, one with the center of the hole at a position of 9 mm from the bottom of the pin, as indicated in Fig. 2(k), and one with a lower position of 8 mm, in which not the centered but the upper region of the window is in the measurement position.

D. Copper capillary for high pressure freezing

While cryogenically protected biological tissue can be mounted on a tip pin version and gradually frozen,[27] this is not easily applicable to samples like suspensions of cells. This is especially true when preservation in a near native state is desirable. Freezing liquids in glass capillaries is also problematic because of the small thermal conductivity of glass. Here we present a solution allowing high-pressure freezing (Leica EM PACT2, HPM 100 and ICE) of liquid sample suspensions filled in copper tubes (Leica). These copper tubes

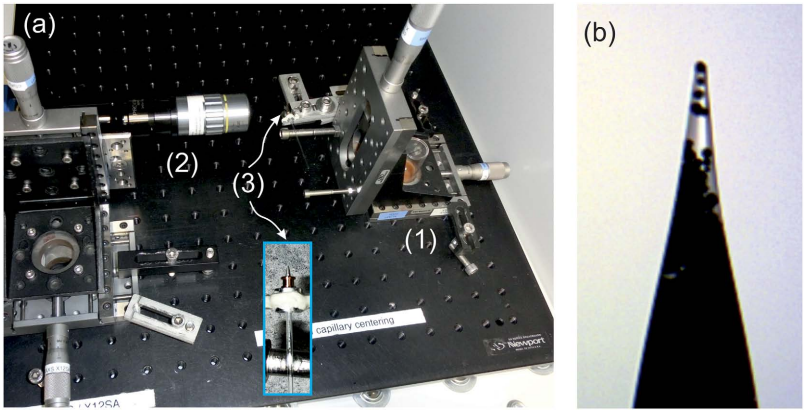

FIG. 5. Mounting a capillary. (a) Mounting mechanics with (1) a manual xy stage where the end of the capillary is resting. This allows manipulating the position of the tapered glass capillary. The position of the tip is observed by a light microscope (2). The capillary is mounted in a capillary pin inserted in a receptor mounted at a fixed position (3). Curing can be done in a controlled way using UV curing adhesive. (b) A light microscopy image of a powder material in a tapered capillary. The tip diameter in the presented case is approximately 15 μm.

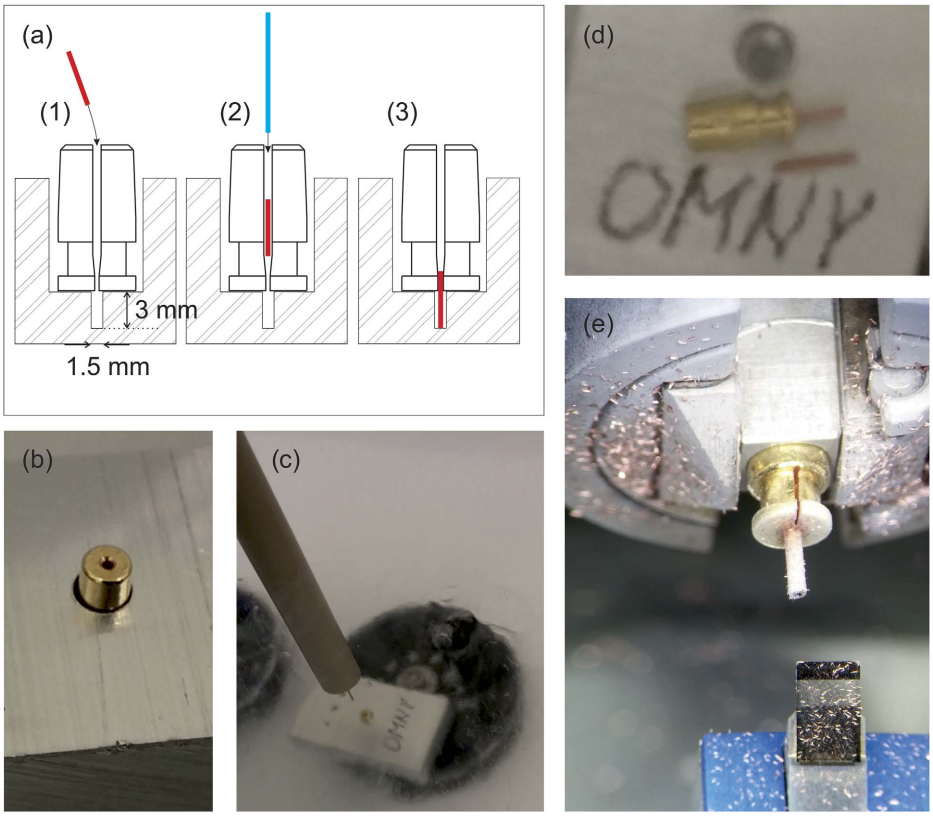

FIG. 6. (a) Schematic of the fixing procedure for the cryo copper tubes, (b) photograph of a pin in the mounting tool. (c) Punching the copper tube to the tip of the pin under liquid nitrogen, (d) a punched tube in a pin under liquid nitrogen with another copper tube next to it, (e) trimming a pin in a cryo ultramicrotome using a diamond knife.

have an outer diameter of 0.65 mm, an inner diameter of 0.35 mm, and a length of approximately 17 mm. After high-pressure freezing and cut-out removal of the copper tube from the perforate steel envelope, the tubes measure approximately 6 mm in length and require mounting in a pin and trimming to dimensions suitable for the measurement. The pin depicted in Figs. 2(l)–2(n) was designed for this case. It offers a 0.7 mm hole in the bottom, where the frozen tube can be inserted. An additional slit allows squeezing the upper region gently, which reduces the 0.7 mm diameter creating a holding spring to snugly hold the copper tube. For mounting the tubes, a pin is placed upside down in a mounting block immersed in liquid nitrogen [Figs. 6(a-1) and 6(b)]. A copper tube is inserted in the back of the pin and then punched downwards to stick out as a tip by a hard metal cylinder [diameter 0.6 mm, Figs. 6(a-2) and 6(c)]. The mounting block allows the tube to stick out by 3 mm, such that the end of the tube is close to the measurement position [Fig. 6(a-3)]. The mounting block has mechanical play on the side of the pin and copper tube such that it cannot get mechanically stuck. Figure 6(d) shows two high-pressure frozen tubes, with one already mounted on a pin. Then, the sample including the copper tube can be further trimmed in a cryo ultramicrotome to the final sample size [Fig. 6(e)].

III. PIN ACCESSORIES AND HANDLING

A. Sample storage and cryogenic sample transfer

Protecting OMNY pins with valuable mounted samples for storage and during transportation is essential for success. We have therefore developed custom containers, both for room temperature and for cryogenically prepared samples. For the latter, samples must remain under cryogenic conditions after sample freezing until a measurement is performed.

For the room temperature samples, pins fit well into standard plastic boxes available from Plano GmbH (Article G3626) as depicted in Fig. 7(a). We developed cushioned cases for storage and transportation as can be seen in Figs. 7(b) and 7(c). The storage and transportation of cryogenic samples is more challenging and required more sophisticated solutions. Figure 7(d) shows a storage case that we developed for cryogenic storage. In contrast to other cases, in which pins are mounted in matching conical receptors, the various holes as shown in this storage box are cylindrical with a diameter of 3.3 mm such that the pins have mechanical play. Figure 7(e) shows an open storage box in liquid nitrogen that is loaded with many samples. A rotatable disc is mounted in the center, ensuring that the pins do not fall out of the storage positions. When rotating the disk, individual pins can be released and taken out with tweezers. For storing, the box is closed by a metal cover that is fixed with screws. The outer diameter of the box is 57 mm. For storing and transportation, the box fits in standard dry shippers (Taylor-Wharton CX-100).

First results of measurements performed at cryogenic conditions in the OMNY instrument are presented elsewhere.[23,27] While in the case of Ref. 23, the sample was transferred to the vacuum chamber of OMNY at room temperature, the cryogenic samples of Ref. 27 required cryogenic sample transfer. The OMNY instrument is operated in

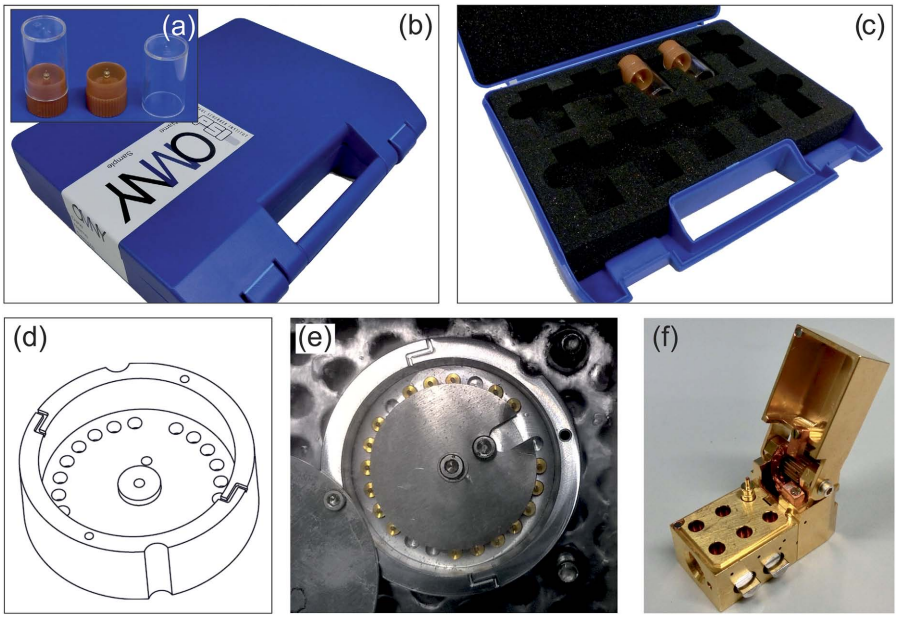

FIG. 7. [(a)–(c)] Storage and transportation of OMNY pins at room temperature. [(d) and (e)] A storage container for cryogenically fixed biological samples. (f) Transfer block for up to six OMNY pins compatible with the Leica VCT100 loadlock system.

vacuum and is equipped with a loadlock system based on the VCT100 from Leica Microsystems. While Leica offers various specimen holders, we developed a transfer block for pins [Fig. 7(f)]. The transfer blocks are relatively rich in mass to maintain cryogenic temperatures during transfer, in which no active cooling is performed. However, used as a

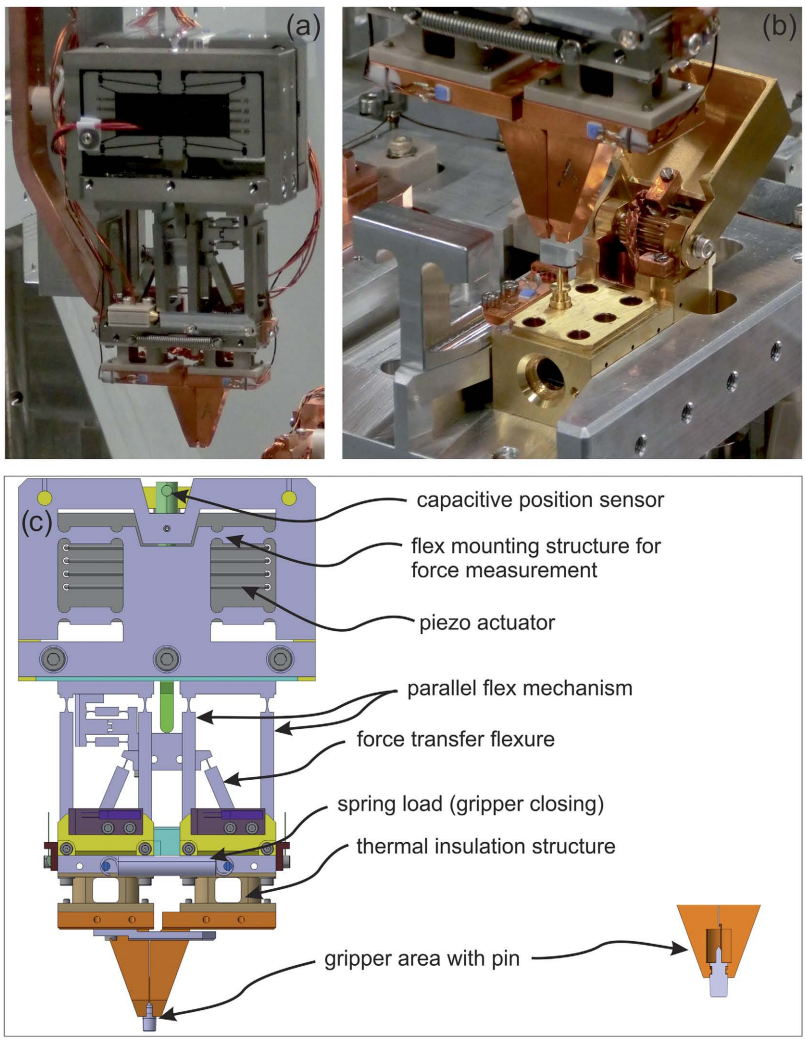

FIG. 8. A flexure based gripper for automatic changing of OMNY pins. (a) A photograph of the gripper, (b) a photograph of the gripper during an unmounting process, see also Movie 1 of the supplementary material. (c) The CAD image of the gripper structure with its individual components.

sample holder directly, they are undesirable for fast sample scanning. Therefore, the transfer block and loadlock are only used to transfer up to six pins to a cryogenic parking space in the vacuum chamber of OMNY. The individual samples are loaded to the transfer block under liquid nitrogen and subsequently protected from contamination and thermal radiation by a cover that is implemented in the transfer block. The transfer of individual pins inside the OMNY instrument is achieved using a cryogenic sample gripper as described in Sec. III B.

B. Automatic sample changer

In many cases, it can be beneficial to load sample pins automatically for a measurement. Especially for cryogenic setups operating in vacuum, this is an essential requirement.[7,12] Here we present a gripper mechanism that, when mounted on a motorized xyz stage, can pick and mount individual pins from a sample storage such as the transfer block depicted in Fig. 7(f). Figure 8(a) shows a photograph of the gripper which is entirely based on a flexure design. A sectional sketch can be seen in Fig. 8(c). The device is operated by a piezoelectric actuator that is pushing onto a force transfer flexure. A downward motion will open the parallel flexure based mechanism. The gripping force itself is controlled by a spring pre-load only, and in a zero voltage state, the gripper is naturally closed. The gripping region is thermally insulated using a peek structure. This allows conductive cooling of the gripping plier when attached to a cold copper braid.

Depending on the manufacturing accuracy of the pins, the required stage positions for mounting a pin on a receptor can slightly vary from batch to batch. Therefore, when mounting a pin, the gripper is not operated based on pre-defined positions. Instead, it is connected to the xyz stage via a strong flexure structure that is used in combination with a capacitive position sensor as a force gauge. When a pre-defined mounting force of approximately 2 N is reached, the mounting process stops, and the pin is released.

Figure 8(b) shows the gripper on top of a sample transfer block installed at the sample parking region of the OMNY instrument. Movie 1 of the supplementary material shows the mounting process of a pin in such a sample transfer block (commissioning/open vacuum chamber).

IV. FIRST IMAGING OF HIGH-PRESSURE FROZEN BIOLOGICAL SAMPLES

For demonstration purposes, we prepared a sample of single-celled green alga samples (*Chlamydomonas reinhardtii* 137c wild type, obtained from the Chlamydomonas Genetic Center) that were cultured as previously described in Tris–acetate–phosphate (TAP) medium.[31] The sample (35 ml) was centrifuged for 5 minutes at room temperature. The supernatant was carefully decanted, and the sample pellet was re-suspended in approximately 3 ml of TAP medium. Approximately 3 μl of the re-suspended liquid sample was pipetted onto a piece of Parafilm® and a fine needle was used to draw the sample through a copper tube held in a perforate steel envelope (all components by Leica Microsystems GmbH), for subsequent high-pressure freezing achieved at −196 °C and ~2000 bars within 20 ms.[32] After mounting the tube in the OMNY pin and trimming the sample in a cryo-ultramicrotome, ptychographic tomography data were collected at the coherent small-angle x-ray scattering (cSAXS) beamline at the Swiss Light Source at the Paul Scherrer Institut in Villigen, Switzerland, using the OMNY instrument. The photon energy used was 6.2 keV. To define the X-ray beam on the sample, a 220 μm-diameter Fresnel zone plate with 60 nm outermost zone width was used.[33] The sample was placed 2.2 mm after the focus where the beam had expanded to about 7.5 μm. 1000 projections with a field of view of 70 μm × 12 μm were recorded and reconstructed as described in Ref. 27. The

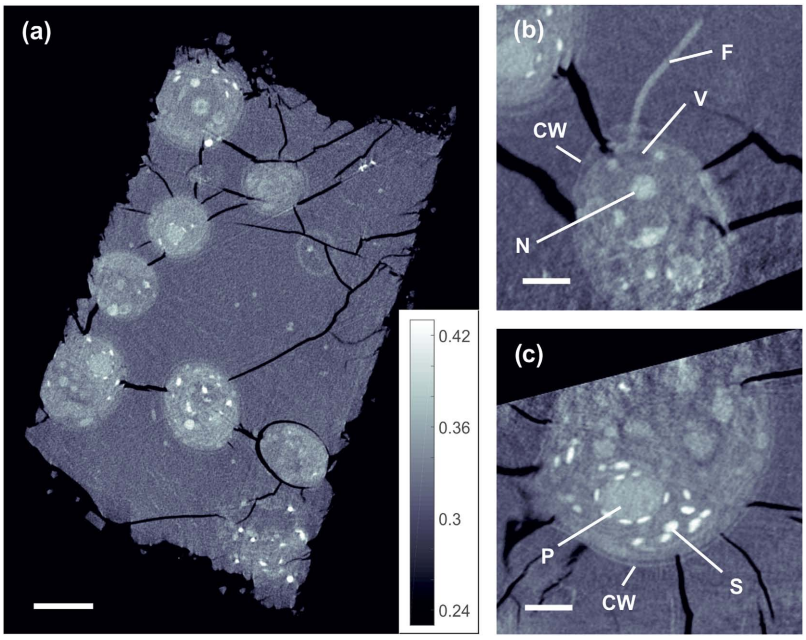

FIG. 9. Ptychographic tomography of high-pressure frozen *Chlamydomonas* solution. (a) Orthoslice through entire measured volume with a thickness of 38.86 nm equal to the voxel size. [(b) and (c)] The average of 5 slices along specific planes in the 3D volume in order to identify some organelles in two different cells: cell wall (CW), nucleolus (N), flagellum (F), vacuole (V), pyrenoid (P), and starch grain (S). The regions on the lower part of (b) and on the top part of (c) lay outside the ptychographic field of view in the scan, which explains the loss of image quality in those regions. Gray scale indicates electron density ($Å^{-3}$). The scale bar is 5 μm in (a) and 2 μm in (b) and (c).

points of the scan were positioned following a Fermat's spiral trajectory[34] with an average spacing of 2 μm, resulting in 207 positions per projection. The exposure time per point was 0.1 s. We estimate that the dose deposited on the specimen for this measurement was 2×10^7 Gy. The resolution was evaluated by the Fourier shell correlation of two subtomograms, each of them obtained from half of the angular projections, as described in Ref. 16, compared with the half-bit threshold.[35] In this way, we estimated an isotropic resolution of about 100 nm in 3D within a volume corresponding to one of the cells.

Figure 9 shows several reconstructed slices where various components of the cells can be identified. The sample did not contain any cryogenic protectant, which caused the formation of large cracks likely during the trimming process. Nonetheless, the image quality improved significantly by high-pressure freezing as compared with previous attempts when glycerol was chosen as a cryoprotectant and a cell solution was plunge-frozen into liquid ethane.[36] Especially notable is the first-time visualization of the flagella of the *Chlamydomonas* cells. We suspect that in previous attempts the cells reacted to that specific cryoprotectant and/or were not thoroughly frozen in a vitreous manner, thereby causing damage to the flagella and/or flagellar retraction. Because ptychographic tomography provides quantitative electron density contrast,[13,36] it is possible to estimate the mass density of different organelles by analyzing the grayscale histograms in different sub-volumes of the dataset. In Table I, we list the measured mass densities obtained by fitting Gaussian curves in small sub-volumes within different organelles in the cell. For this estimate, we assumed a molar mass of 1.85 g/mol, which is the average between the smallest molar mass and the largest molar mass expected for biological tissue, namely, water (1.80 g/ml) and chromatin (1.90 g/mol), respectively.[36] By assuming this, we estimate that the maximum uncertainty in the conversion from electron density to mass densities is about 6%. The values obtained in our analysis generally agree with previous mass density values measured in *Chlamydomonas* cells when prepared by plunge freezing in liquid ethane.[36] We note that in this earlier work, mass densities with less uncertainty in the mass density conversion were obtained by refining the estimate of their compositions, which was not pursued here.

TABLE I. Measured densities in different organelles within high-pressure frozen *Chlamydomonas*. Values were obtained from a Gaussian fit to histograms in subvolumes within the different organelles, and the center and the standard deviation are given. For comparison, the standard deviation in a subvolume within air was found to be 0.008 $Å^{-3}$ or 0.02 g/cm^3.

Organelle	Electron density ($Å^{-3}$)	Mass density (g/cm^3)
Nucleolus	0.368 ± 0.014	1.13 ± 0.04
Vacuole	0.310 ± 0.009	0.95 ± 0.03
Cytoplasm	0.333 ± 0.009	1.02 ± 0.03
Pyrenoid	0.369 ± 0.008	1.13 ± 0.04
Starch grain	0.424 ± 0.019	1.30 ± 0.04
Ice matrix	0.313 ± 0.008	0.96 ± 0.02

V. CONCLUSION

We have developed and presented a versatile sample pin concept for tomographic measurements at the nano-scale for various sample types. The conical pin base offers a high mechanical mounting stability. The pins are lightweight and thus compatible with fast scanning microscopy stages. Their high thermal conductivity and excellent contact makes them ideal for cryogenic experiments and also for future thermal *in situ* experiments. The reproducible mounting due to the conical base simplifies the setting up of measurements. We presented several pin types and further versions are in development, for example, to mount high-pressure frozen tissues contained in discs. The supplementary material offers various manufacturing drawings of the pins that are not limited to scanning X-ray tomography but may also be useful in other instrumentation projects.

SUPPLEMENTARY MATERIAL

See supplementary material for the manufacturing drawings of various pin variants which are available in pdf format. Dimensions are in mm.

ACKNOWLEDGMENTS

We thank ScopeM, the scientific center for optical and electron microscopy of ETH Zürich, for providing access to the xenon FIB/SEM (Tescan, Fera3) and Takashi Ishikawa and Dennis R. Diener for providing the *Chlamydomonas* samples. This work was supported by the SNF R'Equip (Project No. 145056). Ptychography data were collected at the coherent small-angle x-ray scattering (cSAXS) beamline at the Swiss Light Source at the Paul Scherrer Institut in Villigen, Switzerland, using the OMNY instrument.

[1] W. A. Kalender, "X-ray computed tomography," Phys. Med. Biol. **51**, R29–R43 (2006).
[2] A. J. Koster *et al.*, "Perspectives of molecular and cellular electron tomography," J. Struct. Biol. **120**, 276–308 (1997).
[3] E. L. Ritman, "Current status of developments and applications of micro-CT," in *Annual Review of Biomedical Engineering*, edited by M. L. Yarmush, J. S. Duncan, and M. L. Gray (Annual Reviews, Palo Alto, 2011), Vol. 13, pp. 531–552.
[4] D. Attwood, "Microscopy - nanotomography comes of age," Nature **442**, 642–643 (2006).
[5] E. Nazaretski *et al.*, "Design and performance of a scanning ptychography microscope," Rev. Sci. Instrum. **85**, 033707 (2014).
[6] W. L. Chao, B. D. Harteneck, J. A. Liddle, E. H. Anderson, and D. T. Attwood, "Soft x-ray microscopy at a spatial resolution better than 15nm," Nature **435**, 1210–1213 (2005).
[7] S. Chen *et al.*, "The bionanoprobe: Hard x-ray fluorescence nanoprobe with cryogenic capabilities," J. Synchrotron Radiat. **21**, 66–75 (2014).
[8] G. Schneider *et al.*, "Three-dimensional cellular ultrastructure resolved by x-ray microscopy," Nat. Methods **7**, 985–987 (2010).
[9] M. A. Le Gros, G. McDermott, and C. A. Larabell, "X-ray tomography of whole cells," Curr. Opin. Struct. Biol. **15**, 593–600 (2005).
[10] J. J. Deng *et al.*, "X-ray ptychographic and fluorescence microscopy of frozen-hydrated cells using continuous scanning," Sci. Rep. **7**, 10 (2017).
[11] J. J. Deng *et al.*, "Simultaneous cryo x-ray ptychographic and fluorescence microscopy of green algae," Proc. Natl. Acad. Sci. U. S. A. **112**, 2314–2319 (2015).

[12]A. Sorrentino *et al.*, "Mistral: A transmission soft x-ray microscopy beamline for cryo nano-tomography of biological samples and magnetic domains imaging," J. Synchrotron Radiat. **22**, 1112–1117 (2015).
[13]M. Dierolf *et al.*, "Ptychographic x-ray computed tomography at the nanoscale," Nature **467**, 436–439 (2010).
[14]P. Thibault *et al.*, "High-resolution scanning x-ray diffraction microscopy," Science **321**, 379–382 (2008).
[15]M. Holler and J. Raabe, "Error motion compensating tracking interferometer for the position measurement of objects with rotational degree of freedom," Opt. Eng. **54**, 054101 (2015).
[16]M. Holler *et al.*, "An instrument for 3D x-ray nano-imaging," Rev. Sci. Instrum. **83**, 073703 (2012).
[17]M. Holler *et al.*, "X-ray ptychographic computed tomography at 16 nm isotropic 3D resolution," Sci. Rep. **4**, 3857 (2014).
[18]M. Holler *et al.*, "High-resolution non-destructive three-dimensional imaging of integrated circuits," Nature **543**, 402 (2017).
[19]L. K. H. Pallon *et al.*, "Three-dimensional nanometer features of direct current electrical trees in low-density polyethylene," Nano Lett. **17**, 1402–1408 (2017).
[20]C. Donnelly *et al.*, "Element-specific x-ray phase tomography of 3D structures at the nanoscale," Phys. Rev. Lett. **114**, 5 (2015).
[21]J. C. da Silva *et al.*, "Assessment of the 3D pore structure and individual components of preshaped catalyst bodies by x-ray imaging," Chemcatchem **7**, 413–416 (2015).
[22]E. B. L. Pedersen *et al.*, "Improving organic tandem solar cells based on water-processed nanoparticles by quantitative 3D nanoimaging," Nanoscale **7**, 13765–13774 (2015).
[23]B. D. Wilts *et al.*, "Evolutionary-optimized photonic network structure in white beetle wing scales," Adv. Mater. **2017**, 1702057.
[24]M. E. Birkbak, M. Guizar-Sicairos, M. Holler, and H. Birkedal, "Internal structure of sponge glass fiber revealed by ptychographic nanotomography," J. Struct. Biol. **194**, 124–128 (2016).
[25]W. De Boever *et al.*, "Characterization of composition and structure of clay minerals in sandstone with ptychographic x-ray nanotomography," Appl. Clay Sci. **118**, 258–264 (2015).
[26]S. De Angelis *et al.*, "Ex-situ tracking solid oxide cell electrode microstructural evolution in a redox cycle by high resolution ptychographic nanotomography," J. Power Sources **360**, 520–527 (2017).
[27]S. Shahmoradian *et al.*, "Three-dimensional imaging of biological tissue by cryo x-ray ptychography," Sci. Rep. **7**, 6291 (2017).
[28]A. Cuesta *et al.*, "Chemistry and mass density of aluminum hydroxide gel in eco-cements by ptychographic x-ray computed tomography," J. Phys. Chem. C **121**, 3044–3054 (2017).
[29]J. C. da Silva *et al.*, "Mass density and water content of saturated never-dried calcium silicate hydrates," Langmuir **31**, 3779–3783 (2015).
[30]M. S. Nielsen *et al.*, "Ptychographic x-ray computed tomography of extended colloidal networks in food emulsions," Food Struct. **7**, 21–28 (2016).
[31]D. S. Gorman and R. P. Levine, "Cytochrome f and plastocyanin: Their sequence in the photosynthetic electron transport chain of chlamydomonas reinhardi," Proc. Natl. Acad. Sci. U. S. A. **54**, 1665–1669 (1965).
[32]D. Studer, W. Graber, A. Al-Amoudi, and P. Eggli, "A new approach for cryofixation by high-pressure freezing," J. Microsc. **203**, 285–294 (2001).
[33]S. Gorelick *et al.*, "High-efficiency Fresnel zone plates for hard x-rays by 100 keV e-beam lithography and electroplating," J. Synchrotron Radiat. **18**, 442–446 (2011).
[34]X. J. Huang *et al.*, "Optimization of overlap uniformness for ptychography," Opt. Express **22**, 12634–12644 (2014).
[35]M. van Heel and M. Schatz, "Fourier shell correlation threshold criteria," J. Struct. Biol. **151**, 250–262 (2005).
[36]A. Diaz *et al.*, "Three-dimensional mass density mapping of cellular ultrastructure by ptychographic x-ray nanotomography," J. Struct. Biol. **192**, 461–469 (2015).